Planning Non-Entangling Paths for Tethered Underwater Robots Using Simulated Annealing

Seth McCammon and Geoffrey A. Hollinger

Abstract—In this paper we present a simulated annealing-based method for planning efficient paths with a tether which avoid entanglement in an obstacle-filled environment. By evaluating total path cost as a function of both path length and entanglements, a robot can plan a path through multiple points of interest while avoiding becoming entangled in any obstacle. In simulated trials, the robot was able to successfully plan non-entangling paths in an obstacle-filled environment. These results were then validated in pool trials on a SeaBotix vLVB300 underwater vehicle.

I. INTRODUCTION

Offshore energy generation from the motion of the ocean's waves requires the use of fixed emplacements known as Wave Energy Converters (WECs). These devices, which are constantly perturbed by waves, require routine inspections and maintenance to prevent buildup of marine life on the WEC, in addition to mechanical wear and tear. Currently, this is provided either by human divers or by Remotely Operated Vehicles (ROVs), which are teleoperated by a human controller. Control of ROVs is difficult, and automating portions of it, such as navigation to an inspection site, would significantly ease the control burden on the operator.

Underwater inspection involves navigating a ROV or an Autonomous Underwater Vehicle (AUV) on a path which passes through a series of goal points, and returning to the start. At each point of interest along the path, the robot may need to stop to make an observation, or take a sample. A tether connecting the robot to a continuous power supply can extend the mission duration of an AUV indefinitely. The tether also provides a reliable communications link with a base station, and a safety mechanism, preventing the robot from being lost at sea. However, a tether is not without drawbacks. Tethers limit the operational range of the robot, requiring them to stay within some distance of the base station. This range is further limited by the presence of obstacles, as the tether can become wrapped around them. In severe cases of entanglement, where the robot is unable to disentangle itself from the obstacle, it can even prevent the robot's recovery. To address this, we propose a simulated annealing based algorithm which is capable of planning non-entangling paths.

In Section II we discuss related works in the area of tethered robotics, as well as the concept of a homotopy class, a method for describing a curve. Section III describes our algorithm for planning non-entangling paths. In Section IV we discuss the results from testing our algorithm, both in a simulated environment, and in a series of pool tests.
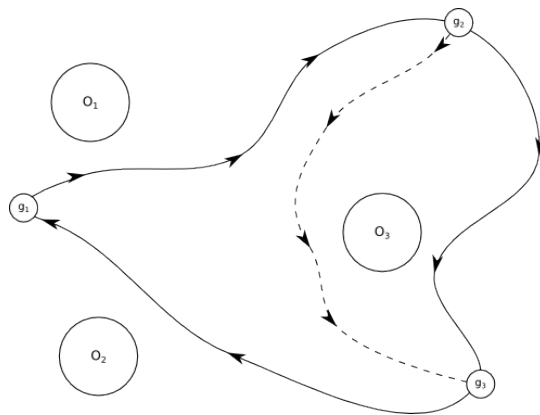

Fig. 1: An example of a trajectory modification which avoids tether entanglement. By modifying the path subsection between g_2 and g_3 (shown with a solid line) to the dotted line, the overall path length may be increased, however, the entanglement with O_3 is eliminated, as O_3 is no longer inside the bound of the trajectory.

II. BACKGROUND

For autonomous underwater inspection tasks, close proximity to obstacles has led previous research, such as that by Kim and Eustice [3], to focus on untethered AUVs to avoid the entanglement risk posed by a tethered vehicle. Existing research in the domain of tethered robots by Kim et al. [4] has focused on planning paths where the length of the tether is the primary constraint, restricting the paths the robot is able to take to its goal. We consider the additional constraint of avoiding entanglement as the robot plans through multiple goal points, by avoiding paths which encircle obstacles. While it is possible for the robot to reverse its path to avoid any entanglement, as was done by Shnaps and Rimon [7] to obtain maximum coverage by a tethered robot, such a behavior can greatly extend the mission duration, reducing the overall area which can be inspected in a reasonable amount of time.

A. Homotopy Classes

A homotopy class describes a set of curves between two points. Two curves share the same homotopy class, (i.e. are homotopic) if they share the same end points and one can be continuously deformed into another without encountering any obstacles. For example, in Figure 1, the dotted and solid curves between g_2 and g_3 do not share the same homotopy class although they do share the same endpoints, since the continuous deformation between them passes through O_3.

In order to characterize homotopy classes, Bhattacharya et al. [2] developed a descriptor, called an H-signature, which
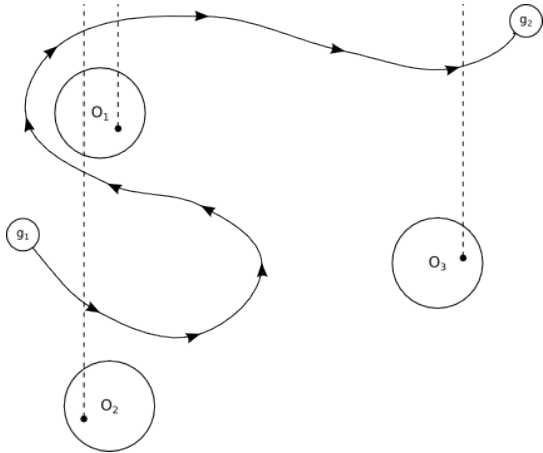
1

Fig. 2: Demonstration of H-Signature Calculation. 1) Representative Points and their rays are constructed within obstacles O_1, O_2, and O_3. 2) Path between g_1 and g_2 is traced and intersections with rays from (1) are recorded. "O_2, O_2^{-1}, O_2, O_1, O_3" 3) H-Signature reduced to "O_2, O_1, O_3"

uniquely describes a homotopy class given a start and end point. The H-signature is computed by selecting representative points inside each obstacle, then drawing a parallel ray from each point. To determine the H-signature of a curve, the curve is traced, beginning at its start point. Each time the trace intersects one of the rays, a symbol corresponding to the ray and direction of intersection is added to the H-signature. This process is demonstrated in Figure 2. A positive crossing of the ray emanating from the nth obstacle is considered to be from left to right, and is denoted as "O_n". The inverse crossing, from right to left is denoted as "O_n^{-1}". The H-signature is then reduced by removing adjacent elements with opposite signs along the same ray. This process is repeated until no more elements can be removed. The resulting H-signature is a homotopy invariant which uniquely identifies the homotopy class of a curve.

III. ALGORITHM

A. Problem Formulation

Our proposed algorithm attempts to find the shortest non-entangling path for a tethered AUV, given a map of the world which contains obstacles $O = \{o_1, o_2, ..., o_n\}$. Each obstacle o_i is defined as a vertical projection from a circle on $\mathbb{R}^2$ to $\mathbb{R}^3$.

The map also contains m goals $G = \{g_1, g_2, ...g_m\}$ where $g_i \in \mathbb{R}^3$. The initial deployment point of the robot is also its first goal g_1. A trajectory T is a complete circuit of these goal points, ultimately returning to the initial deployment point. T consists of two parts. The first is an ordering of goal points G such that the final goal is the same as the initial deployment point, $T_{order} = \{g_1, g_2, ...g_m, g_1\}$. The second component of T is the set of homotopy classes of its sub-paths $h_1, h_2, ...h_m$. The total length of the path, L_T is the sum of all the lengths of the sub-paths, and the total entanglement E_T is the number of obstacles entangled in the tether.

Briefly, we also need to consider the nature of an entanglement. Since the completed trajectory is a loop starting and ending at g_1, obstacles may be divided into an interior and exterior set. Any obstacles in the interior set are considered to be entangled in the tether, while obstacles in the exterior set are non-entangled. There exists a simple test for whether a given trajectory T is entangled in any obstacles. We compute the H-Signature of the entire trajectory T by combining the H-Signature of each of its sub-paths, and then reducing the combined H-Signature as described in Section II-A.

We seek to plan a trajectory T which satisfies the following:

$$T^* = \underset{T}{\text{argmin}}\{L_T | \textit{H-Signature}(T) = \emptyset\}. \qquad (1)$$

We assume that the length of the tether is large compared to the size of the environment, and so it imposes no constraint on the configuration space of the AUV. The problem can be seen as an extension of the Traveling Salesman Problem (TSP), with the additional constraint that the path be non-entangling. We propose a simulated annealing based method which approximates the optimal solution.

B. Simulated Annealing

Simulated annealing is a stochastic optimization algorithm, which performs search in multidimensional space and is robust to entrapment in local optima [5]. Initialized with some random state, x, at each iteration of the algorithm, a successor state x' is generated. As a successor state, x' is created by mutating x through some function. This successor state is compared to the previous state with some evaluation function. If the mutated state has the higher score, it becomes the new state. If it has a lower score, it becomes the new state with the probability shown in Equation 2:

$$p = e^{-(s-s')/\theta}, \qquad (2)$$

where s and s' are the scores of the state and mutated state, θ is the temperature, which decreases over time, making it less likely that an inferior state becomes the successor state.

We initialize the trajectory with a random ordering of the goal points. The path between each consecutive pair of goal points (g_i, g_{i+1}) is planned using A*. During the mutation step of the simulated annealing process the first and last points in this trajectory remain fixed, building on the assumption that the robot is tethered to some fixed base station. At each iteration of the optimization process, a trajectory can undergo one of the two types of mutations chosen at random. The first of these, goal-swapping, swaps the order of two goals on the trajectory.

$$T' = \{g_1, ..., g_{i-1}, g_{\mathbf{j}}, g_{i+1}, ..., g_{j-1}, g_{\mathbf{i}}, g_{j+1}, ..., g_1\}.$$

This mutation can either raise or lower the overall trajectory length and entanglement of the path. To ensure that the resultant path is entanglement-free, we use a second method of mutation, path-inversion. During path-inversion, a subsection of the trajectory between a pair of adjacent goal points is inverted around an obstacle without altering the order of

2
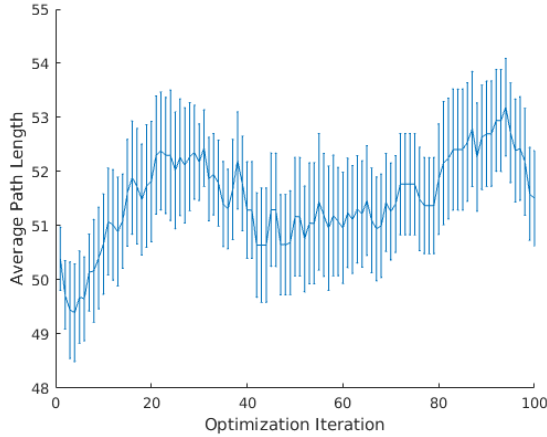
(a) Path length at each iteration while running simulated annealing
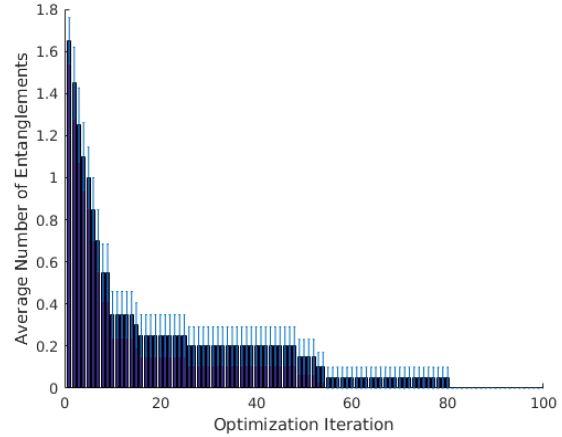
(b) Number of entanglements at each iteration while running simulated annealing

Fig. 3: Average Path Length and Entanglement for a sample path. The configuration of obstacles and goals is the same as shown in Figure 5. Averages are taken over 20 trials. As the number of optimization iterations increase, the number of entanglements rapidly decreases, while the overall path length remains roughly constant. Initial marginal increases in path length are a result of taking longer paths to eliminate entanglements.

the goal points. The subsection of the path is re-planned through an additional sub-goal placed on the opposite side of an obstacle. This inversion alters the homotopy class of the subsection. The result of a path-inversion mutation is shown in Figure 1.

Each trajectory is evaluated by a cost function shown in Equation 3, which evaluates each trajectory on both its entanglement and its overall length:

$$C(T) = k(E_T + 1) * L_T. \tag{3}$$

E_T is the number of obstacles which are entangled by the trajectory T, L_t is the total length of the planned trajectory, and k is a constant factor. In testing, we found that using a large value for k caused the algorithm to eliminate entanglements more quickly.

IV. EXPERIMENTAL TESTING

A. Simulation

Our algorithm was tested in simulation in both randomly generated environments and environments representative of likely deployment locations. The representative environments were modeled on optimal Wave-Energy-Converter layouts developed by Beels et al. [1]. The randomly generated worlds had between 5 and 10 obstacles and between 5 and 10 goals distributed uniformly in the world. In a series of simulated trials, our entanglement-aware planner was compared against a Greedy-TSP planner and a Greedy Backtracking planner. The Greedy-TSP planner selects the closest goal which it has not travelled to at each step. The Greedy Backtracking planner also travels to the closest goal, but then retraces its path back to the start position, ensuring no entanglements. Our method found paths which were on average longer than the greedy planner. However, these paths eliminated all entanglements,
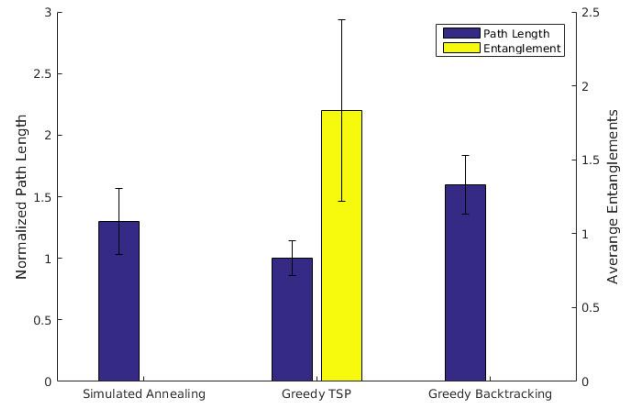

Fig. 4: Comparison of simulated annealing approach with Greedy-TSP and Greedy-Backtracking baseline.

while the greedy solver, having no explicit representation of the obstacles, typically had a large number of entanglements.

B. Pool Trials

The tether behavior was not explicitly modelled in the simulator. Instead, we relied on the assumption that the tether was flexible, and would follow the path of the vehicle. The only way that an entanglement could occur, then, is when the robot's path completely encloses one or more of the obstacles. In order to test this, we implemented the planners on a SeaBotix vLBV300 underwater vehicle [6] equipped with the Greensea INSpect GS3 Inertial Navigation System, a Teledyne Explored DVL, and a Tritech Gemini multibeam sonar. The SeaBotix vehicle can be controlled via a series of waypoints provided through a Robotic Operating System (ROS) interface with a command station.
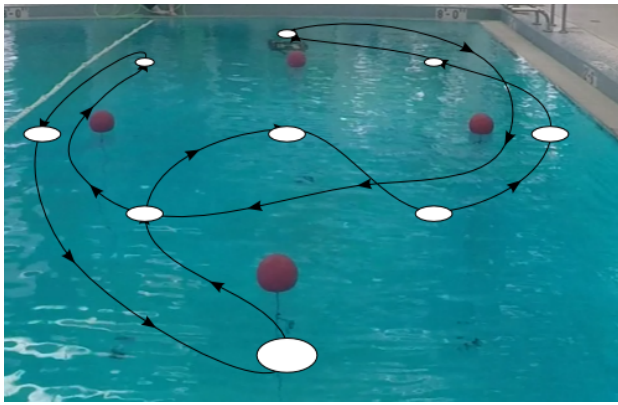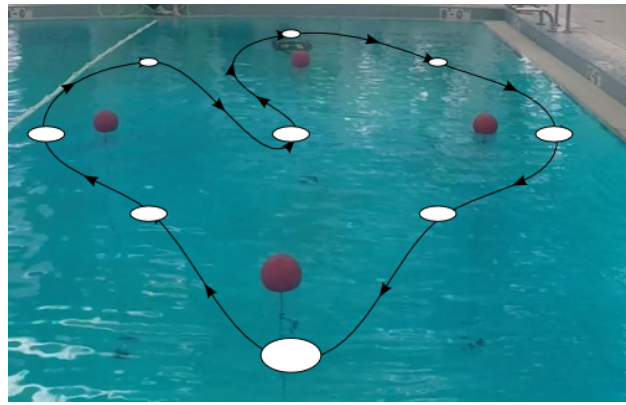
(a) Non-Entangling Path   (b) Greedy Path

Fig. 5: An example obstacle and goal layout for a tethered vehicle. The white circles represent goal locations (all of which lie on the water's surface). The red buoys act as obstacles and indicators of entanglement. The black line shows the planned path for the AUV, and the direction of travel along that path.

Fig. 6: Seabotix vLBV300 Underwater Vehicle

We conducted a series of field trials in two different buoy configurations, a sample of which is shown in Figure 5. The robot was tasked with planning a route which passes through each of the white goal points. Figure 5a shows a route planned by the vehicle using our non-entangling method. The path shown in 5b shows a path through the goals planned by the greedy planner. In these trials, we observed that the tether became entangled when the robot completed an encirclement of an obstacle, but when performing our non-entangling path, the obstacles did not become entangled.

V. CONCLUSION AND FUTURE WORK

In this paper we demonstrated a method allowing a tethered AUV to plan and execute paths which avoid tether entanglement in an obstacle-filled environment. In simulated trials, we found that our method plans longer paths than a greedy TSP solution. However, these paths eliminated all entanglements. Furthermore, these paths were consistently shorter than the naive non-entangling paths. Our method was then tested on the SeaBotix vLBV 300 in a pool, where it was successfully able to navigate the obstacle field. A sample path the vehicle executed is shown in Figure 5.

This work is still ongoing, as we plan to extend our algorithm to three dimensional environments, and use a sampling-based planner to improve the algorithm's performance, particularly in larger environments. Further future directions for this work is to incorporate the affects of disturbances to the tether, such as offshore currents or waves, and to test in environments where the length of the tether does impose a constraint on the motion of the AUV.

REFERENCES

[1] C. Beels, P. Troch, J. Kofoed, P. Frigaard, J. Kringelum, P. Kromann, M. Donovan, J. Rouck, and G. Backer. A methodology for production and cost assessment of a farm of wave energy converters. *Renewable Energy*, 36(12): 3402 – 3416, 2011.

[2] S. Bhattacharya, M. Likhachev, and V. Kumar. Topological constraints in search-based robot path planning. *Autonomous Robots*, 33(3):273–290, 2012.

[3] A. Kim and R. Eustice. Pose-graph visual slam with geometric model selection for autonomous underwater ship hull inspection. In *proc IEEE/RSJ International Conference on Intelligent Robots and Systems, 2009.*, pages 1559–1565.

[4] S. Kim, S. Bhattacharya, and V. Kumar. Path planning for a tethered mobile robot. In *proc IEEE International Conference on Robotics and Automation, 2014*, pages 1132–1139.

[5] S. Kirkpatrick, C. D. Gelatt, and M. P. Vecchi. Optimization by simulated annealing. *Science*, 220(4598):671–680, 1983.

[6] *vLBV Operator's Manual*. SeaBotix Inc., 2877 Historic Decatur Road STE 100, San Diego, CA 92106 USA, revision l edition, jun 2014.

[7] I. Shnaps and E. Rimon. Online coverage by a tethered autonomous mobile robot in planar unknown environments. *IEEE Transactions on Robotics*, 30(4):966–974, 2014.